Article

Chemical Structure Evolution of Thermally Altered Coal during the Preparation of Coal-Based Graphene and Division of Thermally Altered Zone: Based on FTIR and Raman

Ruiqing Li, Yuegang Tang,* Xiaoxia Song, Shaoqing Wang, Qili Che, and Cong Chen

Read Online

ACCESS | Metrics & More | Article Recommendations

ABSTRACT: A suite of coal samples near a diabase dike was collected to investigate the structural and functional group evolution of a series of carbon materials prepared from thermally altered coals, explore the influence of thermal metamorphism distance on the structure of coal and its carbon material products, and divide the thermally altered zones. Using Fourier transform infrared and Raman studies, it was found that after demineralization, the aromatic parameters f_{ar}^{H} and I of the coal structure slightly increase, while the aliphatic parameters CH_2/CH_3 and oxidation parameter $'C'$ slightly decrease, and the degree of order of the coal structure increases. Graphitization can greatly improve aromatic parameters, eliminate aliphatic structures, and enhance orderliness. However, after oxidation and reduction, the aromatic parameters and ordering degree of graphene decrease. Except for the sample closely attached to the dike, the coal-based graphene yield of the other samples first decreases and then stabilizes with the increase of distance from the dike, which is consistent with the trend of changes in the reflectance of raw coal. The thermally altered distance affects the structural changes of coal and carbon material products. The coal attached to the dike has been damaged and polluted, and the aromaticity and orderliness of the prepared carbon material products are relatively poor. The aromaticity and orderliness of coal-based products prepared from other thermally altered coals are relatively high and increase with the closer the thermally altered distance. Based on the characterized parameters of coal samples and products with distance from the dike, the sampling area is divided into four zones, including abnormally altered zone, normal altered zone, transition zone, and original coal zone. Among them, the yield and quality of coal-based graphene prepared from coal in the normal altered zone are the highest, an ideal raw material collection area for making coal-based graphene.
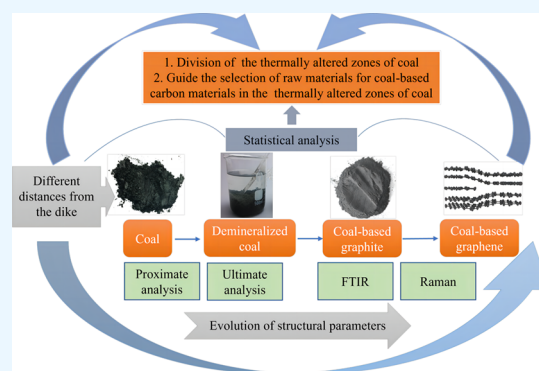
1. INTRODUCTION

As a high-value-added carbon material with excellent properties, coal-based graphene is an important industrial chain of the coal industry and has great application potential in many fields.[1−3] As a carbon source with large reserves and a rich aromatic structure, coal is an ideal raw material for the preparation of coal-based carbon materials.[4,5]

At present, research on coal-based graphene is in the exploratory stage, and most of the studies focus on the influence of coal rank, macerals, and minerals on coal-based graphene.[6−9] However, there is little research on the influence of metamorphism on coal-based graphene. Coal metamorphism is a chemical change process of carbon enrichment, dehydrogenation, and deoxidation, accompanied by changes in physical and chemical properties such as porosity and density.[10] The growth and splicing of aromatic structures in coal and the formation of basic structural units (BSU) in the late stage of coalification are the main mechanisms of coal graphitization.[11] Coal with different maturities has different original structures, which will affect graphitization and its graphitic products, and the

metamorphism of coal is an important factor affecting the maturity of coal.[8,9,12,13] Contact metamorphism occurs when the heat source (magma) directly contacts the coal seam, causing the coal seam to alter. The intruded igneous intrusion provides high-temperature and high-pressure conditions for the coal seam and affects the physical and chemical structure of the coal.[14−16] Compared with plutonic metamorphism, coal subjected to thermal contact metamorphism has greater vitrinite reflectance and a higher degree of metamorphism.[17−20] From the perspective of coal petrology and coal quality, the thermally altered zone can be divided into the altered zone and the unaltered zone.[20,21] In a suit of thermally altered coal, there is often a series of mineral changes.[22−24] The formation and
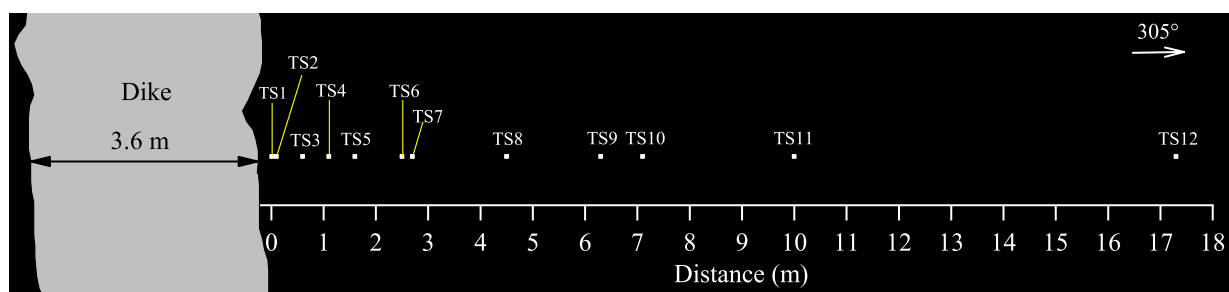
Figure 1. Sampling diagram of the Tashan coal.

evolution of thermally altered coal may follow a slightly different maturation pathway.[25] For the study of coal-based carbon materials, more attention should be given to the molecular evolution of thermally altered coal. In terms of aromatic stripe orientation, lattice stripes become more orderly with the distance from the dike, and the molecular reactivity of coal is enhanced.[26,27] Chen et al.[28,29] divided the evolution of structural parameters of thermally altered coal into three stages and found that two different types of structures, aromatic clusters, and graphite-like structures, could be distinguished in all thermally altered coal samples. This is of great significance for the preparation of coal-based graphene from thermally altered coal.

Fourier transform infrared spectroscopy (FTIR) has always been an important means to study the chemical structure of carbon materials.[30] Li et al. studied the structure of vitrinite in different coal ranks in detail by FTIR, and the pattern of functional group changes in the macromolecular structure in vitrinite was obtained.[31] Jiang et al. studied the pyrolysis behavior and product distribution of Shenmu coal at high heating rates by FTIR, and the pattern of functional group changes in the macromolecular structure in vitrinite was obtained.[32] The relationship between sulfur in coal and coal maturity was studied through FTIR.[33,34] Huan et al. explored the functional group changes of coal-based graphitic products from anthracite with different coal ranks by using FTIR.[6] Raman spectroscopy is widely used in geoscience and materials science. It is one of the important nondestructive analysis methods of coal, char, graphite, graphene, and other carbon materials.[35−38] With increasing coal metamorphism temperature, the graphite band (G-band) becomes the main band, indicating that the molecular structure of high-rank contact metamorphosed coal is close to that of well-crystallized graphite.[39] The Raman characteristics of inertinite and vitrinite in thermally altered coal are significantly different. Li et al. found that the Raman spectral parameters of vitrinite and inertinite macerals are different and predicted the temperature of thermally altered coal when it is intruded. The macerals in thermally altered coal are easy to coked in the samples adjacent to the dike, and the vitrinite would form mesophase spheroids.[40,41]

In this study, we aim to (1) describe the evolution of the structural parameters of coal-based graphitic products from thermally altered coal during the preparation process, (2) investigate the influence of contact metamorphism on coal-based graphitic products, and (3) discuss the division of thermally altered zones according to the parameters of samples and products. This work can provide new insights into the selection of raw materials for coal-based carbon products and the comprehensive utilization of thermally altered coal.

2. EXPERIMENTAL SECTION

2.1. Sample Collection. The Datong Coalfield is in the northern area of Shanxi Province, China. The coal-bearing strata of the Datong Coalfield include the Jurassic Datong, Lower Permian Shanxi, and Upper Carboniferous Taiyuan formations.[42] The Datong Coalfield was intruded by igneous intrusions in both the Indosinian (Late Permian to the end of the Triassic) and Yanshan (Late Jurassic to the Early Cretaceous) periods, forming thermally altered coal.[43,44] Thermally altered coal has characteristics such as high vitrinite reflectance, low volatile matter, high strontium content, high aromaticity and condensation degree, low CH_2/CH_3, and occurrence of thermally altered organic particles with many graphite like structures.[22,28,29,41,44] Due to its high degree of order and aromaticity, thermally altered coal can be used as a raw material for coal-based carbon materials.[28,29,41]

Contact metamorphism mainly occurred in the southeastern and northern central parts of the minefield, and the no. 3 and no. 5 coal seams of the Taiyuan formation are greatly affected. The sampling place is in the 5222 tunnels of the Tashan Coal Mine, where a dike with a width of 3.6 m is exposed, and weathering zones with a width of 0.5 m appear on both sides. The sampling method involved sampling sections according to the distance from the dike. As shown in Figure 1, the interval near the dike is relatively close, and the interval far away from the dike is relatively large. A total of 12 samples were collected for this study.

2.2. Demineralization and Graphitization. To avoid the influence of minerals in the coal samples on the graphitization process and structural analysis of coal-based products,[45] the samples were demineralized in advance. Samples were crushed to 200 mesh. Coal powders were successively treated with HCl, HF, and HNO_3 successively in polytetrafluoroethylene (PTFE) beakers (soaked and stirred in 60 °C ultrapure water for 24 h) to remove minerals in the coal samples.[6,46,47] After washing (washed with ultrapure water until pH = 7) and drying (at 60 °C in a vacuum oven), demineralized samples were obtained and marked with the prefix D.

Five grams of demineralized coal powder was weighed and placed in a graphite crucible, heated to 1000 °C (5 °C/min) for 1 h of carbonization in a graphite furnace under vacuum, rapidly heated (20 °C/min) to 2800 °C and maintained at this temperature for 3 h under an argon atmosphere to prepare coal-based graphite.[48] The coal-based graphite obtained above was marked with the prefix G.

2.3. Preparation of Coal-Based Graphene. Coal-based graphene oxide was prepared according to a modified Hummers' method.[49,50] A total of 68 mL concentrated H_2SO_4 was mixed with 1.5 g of $NaNO_3$ powder and stirred for approximately 10 min until the $NaNO_3$ was completely dissolved. Two grams

Table 1. Maximum Reflectance of Vitrinite, Proximate Analysis and Ultimate Analysis of Raw Coal Samples[a]

sample	distance (m)	$R_{o,max}$ (%)	proximate analysis (wt %)					ultimate analyses (wt %)					H/C (atom)	O/C (atom)
			M_{ad}	A_d	V_{daf}	$S_{t,d}$	C_{daf}	H_{daf}	N_{daf}	$S_{t,daf}$	O_{daf}*			
TS1	0.01	3.71	4.86	21.16	15.18	0.32	87.69	0.98	0.91	0.41	10.01	0.13	0.09
TS2	0.1	3.59	4.34	14.49	7.16	0.56	91.82	1.91	1.31	0.65	4.31	0.25	0.04
TS3	0.6	2.92	2.28	12.77	7.74	0.43	91.18	2.52	1.48	0.49	4.33	0.33	0.04
TS4	1.1	1.82	1.22	12.59	13.52	0.38	89.14	3.51	1.58	0.43	5.34	0.47	0.04
TS5	1.6	1.57	1.15	11.65	21.57	0.61	82.95	5.36	1.40	0.69	9.60	0.78	0.09
TS6	2.5	0.74	1.50	10.70	30.55	0.51	84.74	4.53	1.47	0.57	8.69	0.64	0.08
TS7	2.7	0.85	1.46	9.86	31.10	0.41	84.71	4.75	1.58	0.45	8.51	0.67	0.08
TS8	4.5	0.73	1.82	7.72	38.61	0.50	82.62	5.05	1.56	0.54	10.23	0.73	0.09
TS9	6.3	0.75	1.70	6.97	37.31	0.57	83.54	5.10	1.57	0.61	9.18	0.73	0.08
TS10	7.1	0.73	1.74	9.75	32.35	0.39	83.59	4.64	1.50	0.43	9.84	0.67	0.09
TS11	10.0	0.76	1.44	10.42	39.17	0.41	83.08	5.18	1.50	0.46	9.78	0.75	0.09
TS12	17.3	0.74	1.66	8.06	39.14	0.47	83.02	5.23	1.53	0.51	9.71	0.76	0.09

[a]$R_{o,max}$, maximum vitrinite reflectance; M, moisture; A, ash yield; V, volatile matter; S_t, total sulfur; C, carbon; H, hydrogen; N, nitrogen; O, oxygen; H/C, ratio of hydrogen to carbon atoms; O/C, ratio of oxygen to carbon atoms; ad, air-dried basis; d, dry basis; daf, dry and ash-free basis; *, by difference.

of coal-based graphite were added, and the temperature was kept below 5 °C in an ice bath for 20 min. Then, 10 g of $KMnO_4$ was slowly added to the reaction system and stirred for approximately 30 min to ensure the oxidation effect of $KMnO_4$ on coal-based graphite. The reactants were continuously stirred in a 35 °C water bath for 3 h, and 50 mL of ultrapure water was slowly added to the reaction system. Then, the temperature was raised to 98 °C, and the reactants were stirred for 20 min. After the beaker was removed, approximately 30 mL of hydrogen peroxide (H_2O_2, mass fraction 30%) was added to ensure the complete removal of $KMnO_4$. The obtained reactants were centrifuged at 5000 r/min for 30 min, and the paste was washed to neutral with ultrapure water and dried in a vacuum drying oven at 50 °C for 24 h to obtain coal-based graphite oxide. Graphite oxide was centrifuged after 5 h of ultrasound, and the supernatant solution was freeze-dried to obtain graphene oxide. The coal-based graphene obtained above was marked with the prefix GO.

Approximately 100 mg of coal-based graphene oxide solid and 500 mL of N,N-dimethylformamide ($N_2H_4 \cdot H_2O$) were mixed and were ultrasonicated for approximately 2 h. Two milliliters of $N_2H_4 \cdot H_2O$ were added, and the mixture was incubated in a constant temperature water bath at 95 °C for approximately 5 h. When the reactants were cooled to room temperature, they were washed to neutral with ultrapure water, and the washing solution was tested to ensure that SO_4^{2-} and NO_3^{-1} were not detected. The washed products were freezing vacuum-dried to obtain coal-based graphene. The coal-based graphene above was labeled with the prefix GS.

2.4. Analytical Methods. The maximum reflectance of vitrinite ($R_{o,max}$, %) was determined by a Leitz Orthoplan microscope equipped with a Daytronic mainframe 9005 spectrophotometer based on ASTM Standard D 2798−21.[51] Proximate analyses of coal were determined following ASTM D3173/D3173M-17a, ASTM D3174−12 (2018) e1, and ASTM D3175−20, ultimate analysis was performed based on ASTM Standard D5373-21, and total sulfur analysis was performed according to ASTM D3177−02.[52−56]

3. RESULTS AND DISCUSSION

3.1. Chemical Properties of Coal. The maximum reflectance of vitrinite, proximate analysis, ultimate analysis, the ratio of hydrogen to carbon atoms, and the ratio of oxygen to carbon atoms analysis results are listed in Table 1. The $R_{o,max}$

(%) of the samples is 3.71−0.73%, of which the $R_{o,max}$ (%) of raw coal samples TS1-TS5 (within 1.6 m) is 3.71−1.57%, which is higher than that of other raw coal samples. The ash yield and volatile matter of the TS1-TS5 samples range from 21.16 to 11.65% and 7.16 to 21.57%, respectively, which are also higher than those of the other raw coal samples. TS1-TS5 were classified as thermally altered coal, with an alteration halo of 2 m, and the other raw coal samples were classified as unaltered coal.[22] In the thermal halo, the carbon content and H/C of TS1 are relatively low, and the O/C is the highest, which is caused by the intrusion of material brought by magma. The raw coal samples in the unaltered area are similar regarding the indicators of proximate analysis and ultimate analysis.

3.2. FTIR Results. The FTIR spectrum of carbon materials was divided into four characteristic absorption regions: 700−900 cm^{-1} mainly represents the deformation vibration of C−H substitution in the aromatic ring; 1000−1800 cm^{-1} mainly belongs to the deformation vibration of various oxygen-containing functional groups, CH_2, and CH_3 as well as the expansion vibration of the aromatic ring, 2800−3000 cm^{-1} is generally considered as the expansion vibration absorption region of aliphatic hydrocarbon CH_X, and 3000−3700 cm^{-1} is mainly the absorption vibration region of hydroxyl groups. Combined with the previous research results.[57−60] The main infrared absorption peaks of carbon materials are shown in Table 2.

Figure 2 depicts the normalized FTIR spectra of raw coal samples and graphitic products. The FTIR spectra of raw coal, demineralized coal, coal-based graphite, coal-based graphene oxide, and coal-based graphene are shown in Figure 2a,b, respectively. Figure 2 shows that the types of functional groups contained in all samples and products are similar throughout the FTIR spectrum. There are sharp absorption peaks in the range of 400−600 cm^{-1} of raw coal, mainly caused by Si−O−Si and Si−O bonds, indicating that raw coal contains minerals such as quartz or kaolinite.[61,62] After demineralization, the mineral peak in coal basically disappears, and it appears weaker in coal-based graphite, coal-based graphene oxide, and coal-based graphene. After graphitization, most of the functional group peaks in the spectrum almost disappear and become smooth. Compared with raw coal and demineralized coal, there are no obvious prominent absorption peaks. Even the most sensitive hydroxyl peaks (∼3400 cm^{-1}) in carbon materials are almost invisible in the infrared spectrum of coal-based graphite, and this result is like

Table 2. Assignments of FT-IR Absorption Wave Number in Carbon Materials[57,60]

functional group	peak (cm^{-1})
3630	Free −OH
3560	OH−π hydrogen bond
3350−3470	Self-associating hydroxyl, pyrrole-NH
3250	OH- Ether oxygen bond
3000−3100	Aromatic CH$_X$
2800−3000	Aliphatic CH$_X$
2950−2960	Aliphatic CH$_3$
2920−2930	Aliphatic CH$_2$
1700−1720	Ketones, aldehydes, carbonyls, and carboxyls
1650−1800	C=O groups
1590−1610	Aromatic C=C
1600	Aromatic rings
1440−1455	Aliphatic CH$_x$
1370−1375	Aliphatic CH$_3$
1000−1300	C−O of phenol, alcohol, ether, and ester
700−900	Aromatic C−H out-of-plane bending modes
860	Isolated aromatic H
833 (weak)	1,4-substituted aromatic groups
815	Isolated H and/or two neighboring H
750	1,2-substituted, i.e., 4 neighboring H
700	Isolated or 1,3-substituted aromatic H

Figure 2. FTIR spectra of coal samples and products: (a) raw coal and demineralized coal; (b) coal-based graphite, coal-based graphite oxide, and coal-based graphene.

that of natural graphite.[6] To study the organic structure changes of raw coal and products, according to references,[34,60] the FTIR spectra of raw coal and products are divided into three absorption bands: the aromatic structure absorption band (900−700 cm^{-1}), oxygen-containing functional group absorption band (1800−1000 cm^{-1}) and aliphatic structure absorption band (3000−2800 cm^{-1}). The fitting method of the spectra of all samples is similar; taking the TS6 sample as an example, the curve-fitting procedure is shown in Figure 3.

According to Table 2, peak fitting was performed to obtain the area of each functional group peak by Origin. According to previous refs [34,59,63−66], the calculation of FTIR parameter f_a is

$$f_{ar}^H = 1 - \frac{H_{al}}{H}$$

$$\frac{H_{al}}{H} = \frac{H_{al}}{H_{al} + H_{ar}} = \frac{A_{2800-3000}}{A_{2800-3000} + A_{700-900}}$$
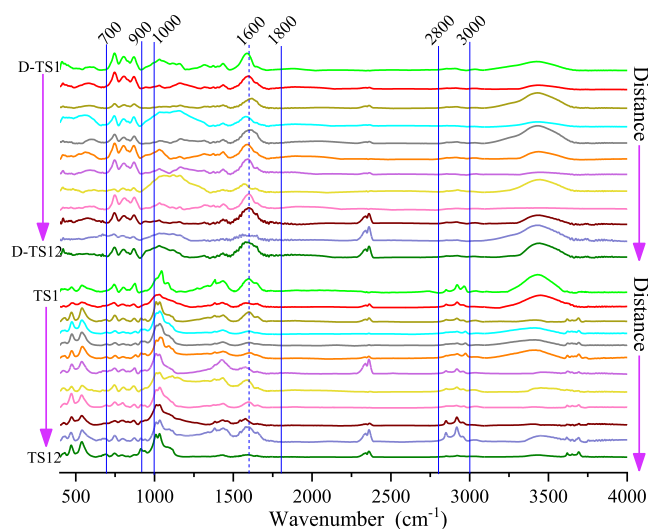
$$f_{ar}^C = 1 - \frac{C_{al}}{C}$$

$$\frac{C_{al}}{C} = \left(\frac{H_{al}}{H} \times \frac{H}{C} \right) / \frac{H_{al}}{C_{al}}$$

where C_{al}/C is the aliphatic carbon fraction, H_{al}/H is the fraction of total hydrogen present as aliphatic hydrogen, H/C is the ratio of hydrogen to carbon atoms calculated from elemental analysis, and H_{al}/C_{al} is the ratio of hydrogen to carbon atoms for aliphatic groups, which is generally taken to be 1.8 for coals.[59]
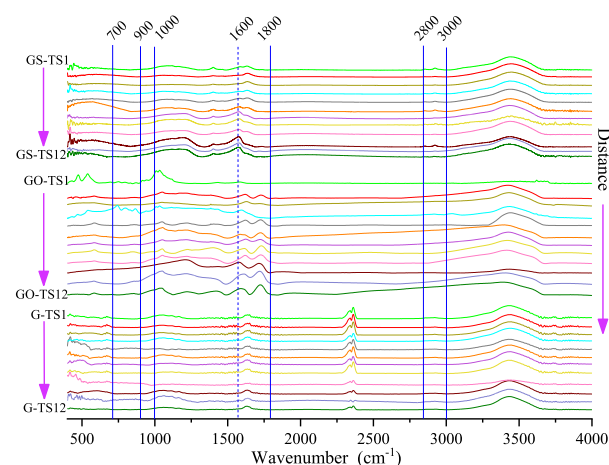
The parameter I also indicate the aromaticity, and the coal rank and can be determined as[64]

$$I = \frac{A_{700-900}}{A_{2800-3000}}$$

where $A_{700-900}$ is the area of 700−900 cm^{-1} and $A_{2800-3000}$ is the area of 2800−3000 cm^{-1}. The degree of condensation (DOC) of aromatic rings can be determined as[34,65]

$$DOC = \frac{A_{700-900}}{A_{1600}}$$

where the 'C' factor is the ratio of C=O groups to C=C groups that is used to indicate the maturation of coal and can be determined as[34,63,66]

$$'C' = \frac{A_{1650-1800}}{A_{1650-1800} + A_{1600}}$$

The $A(CH_2)/A(CH_3)$ ratio was used to estimate the length and degree of branching of aliphatic side chains and can be determined as[32,59,66]

$$\frac{A(CH_2)}{A(CH_3)} = \frac{A_{2915-2940}}{A_{2950-2975}}$$

According to the above formulas, the structural parameters of raw coal, demineralized coal, coal-based graphite, coal-based graphene oxide, and coal-based graphene are calculated (Appendices A1 and A2).

As shown in Figure 4a,b, both f_{ar}^H and I of demineralized coal slightly improved compared with raw coal because a strong acid will destroy the aliphatic long chains in coal and reduce −CH$_2$,
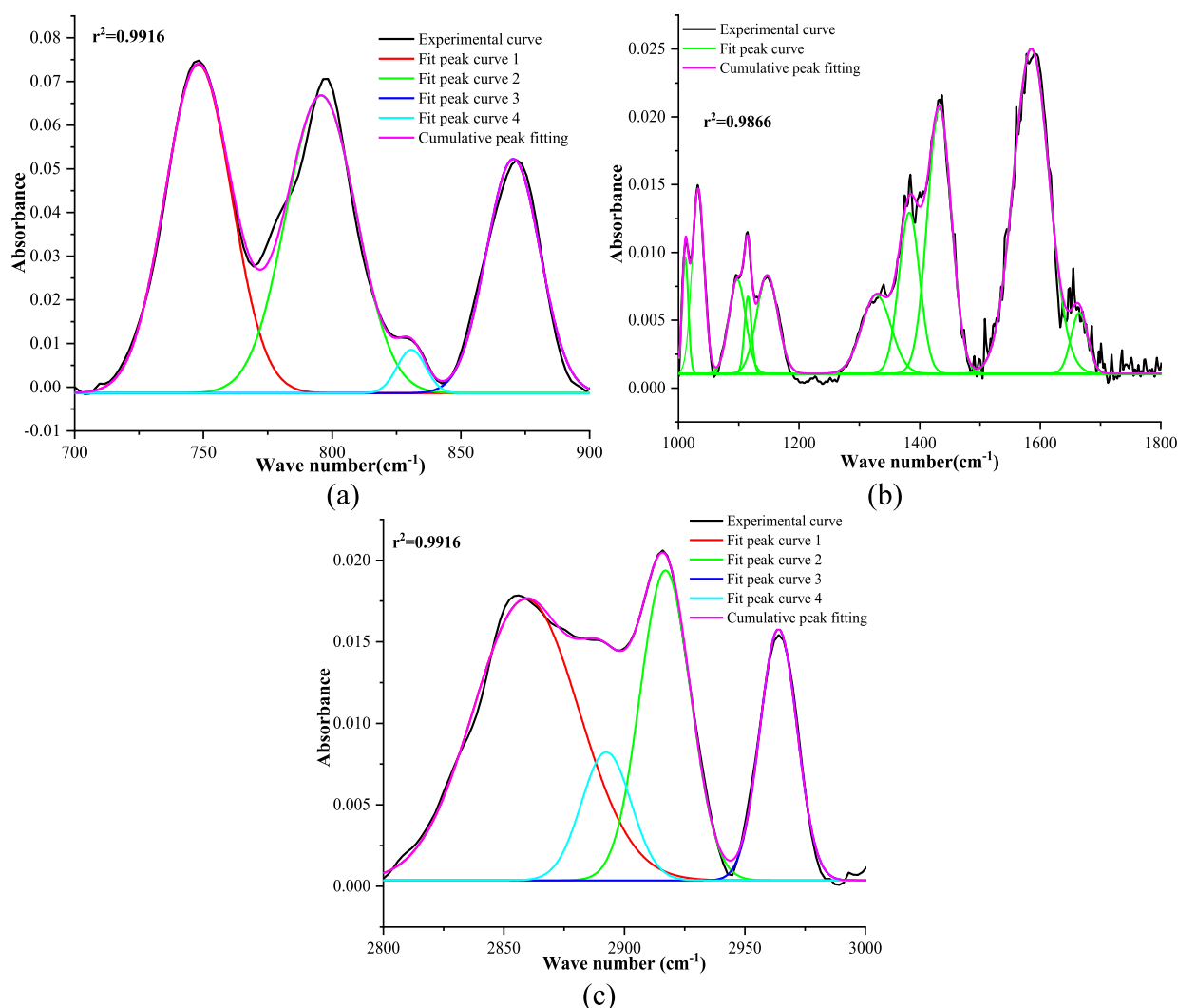
Figure 3. Curve-fitting of the FTIR spectrum of sample TS6 (according to refs 57−60): (a) Absorbance bands of 700−900 cm^{-1}. (b) Absorbance bands of 1000−1800 cm^{-1}. (c) Absorbance bands of 2800−3000 cm^{-1}.

indicating that demineralization is conducive to the graphitization process. After graphitization, due to the disappearance of a large number of aliphatic chains, the f_{ar}^{H} and I of coal-based graphite are significantly higher than those of raw coal and demineralized coal. In the oxidation−reduction process, strong oxidants further cut aliphatic short-chain breaks and reduce −CH$_3$, resulting in a slight increase in f_{ar}^{H} and I of coal-based graphene oxide compared with coal-based graphite. However, the strong reduction has little effect on f_{ar}^{H} and I. This makes the f_{ar}^{H} and I of the graphitized series products maintain a high level, in which f_{ar}^{H} is above 0.9, and the I of coal-based graphene reaches up to 65.23. The aromatization indices f_{ar}^{H} and I of the samples and products change similarly to the distance from the dike. Within 0.1 m, from TS1 to TS2, the f_{ar}^{H} and I of all samples and products have a jump rise. This is because TS1 is close to the rock wall, and the aromatization of the coal structure is not complete due to a large amount of short-term high-temperature heat and exogenous substances from the magma in direct contact. The greater separation distance will buffer the magmatic heat and block exogenous substances from the magma, which is conducive to the aromatization of TS2-TS5 samples and products. Within 0.1−2 m, f_{ar}^{H} and I decreased significantly, indicating that this is a normal thermally altered

reaction within this distance range; that is, with increasing distance from the magma, the aromatic hydrogen rate and aromatization weakened. Within 2−6 m (TS6-TS8), both coal samples and products the f_{ar}^{H} and I are between those of thermally altered coal and original coal, with small fluctuations, showing a transition trend from thermal altered coal to original coal. When the distance is greater than 6 m (TS9-TS12), the values of f_{ar}^{H} and I tend to be stable. The DOC is also an indicator of aromaticity, as shown in Figure 4c. The DOC has a jump rise within 0.1 m; the reason is that the high temperature of the intrusion caused a high degree of condensation of the aromatic rings. The DOC of demineralized coal is slightly higher than that of raw coal, indicating that demineralization is conducive to the improvement of the DOC. The DOC values of raw coal and demineralized coal decrease significantly with the increase of distance within 0.1 to 2 m and decrease slightly within 2−6 m, which also shows that there is a normal thermally altered reaction within 0.1 to 2 m and a transition region within 2−6 m. The DOC of graphitic products decreases slightly with fluctuations within 0.1 to 6 m. For TS6-TS12 (more than 2 m), the DOC of graphitic products is higher than those of raw coal and demineralized coal, indicating that graphitization has little effect on the DOC of high reflectance coal, but it can effectively
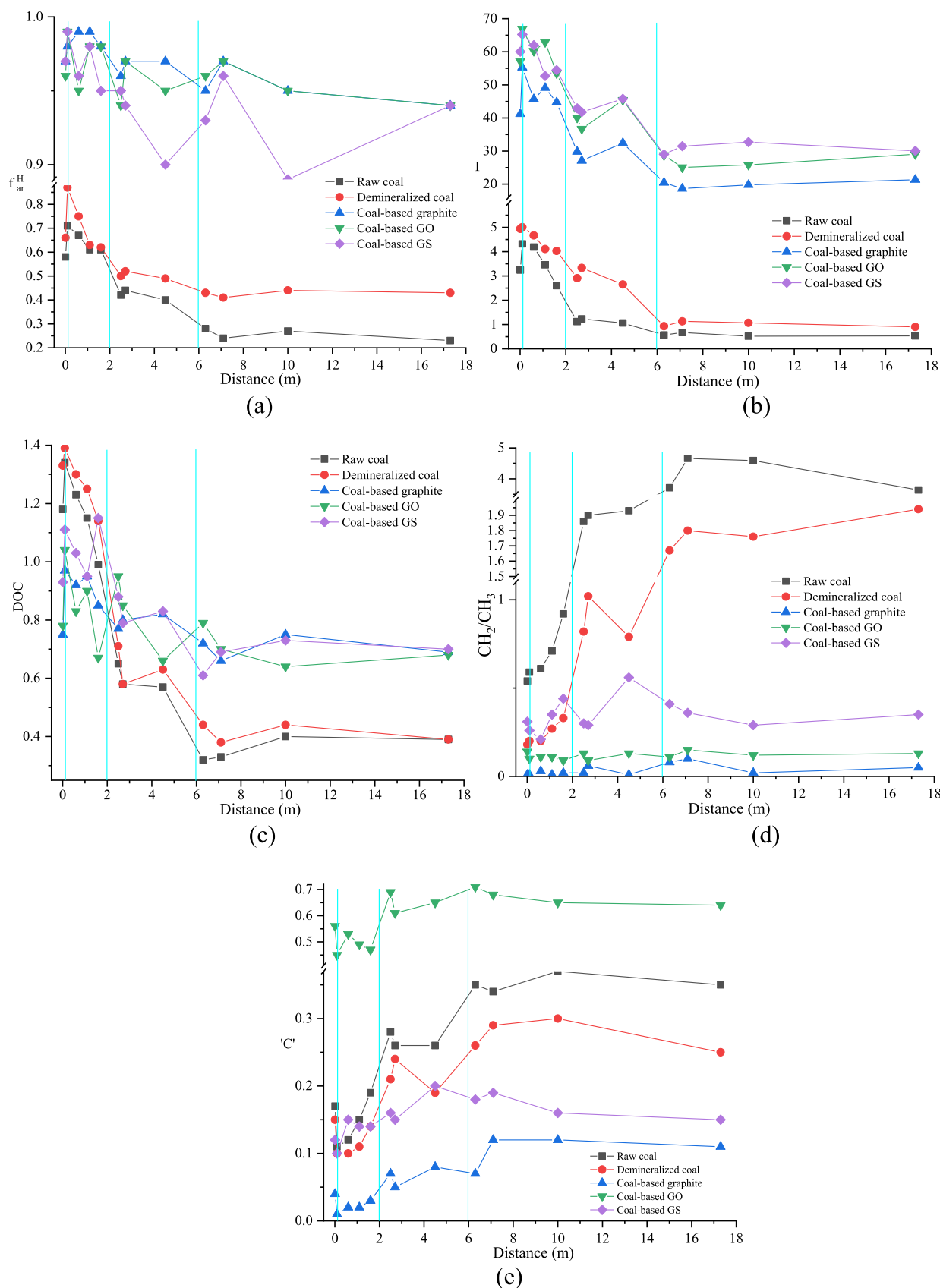
Figure 4. Comparison of the variation in FTIR parameters between coal samples and coal-based products with different distances from the dike: (a) f_{ar}^{H}, apparent aromaticity; (b) I, the relative abundance of aromatic to aliphatic components; (c) DOC, degree of condensation of aromatic rings; (d) CH_2/CH_3, Aliphatic chain length; (e) "C", Oxidation degree.

improve the DOC of low reflectance coal with more aromatic C−H.

Figure 4d shows the correlation of aliphatic structural parameters (CH_2/CH_3) of samples and products with distance from the dike. Within 2 m (TS1-TS5), the aliphatic structural parameters CH_2/CH_3 of both raw coal and demineralized coal increase with distance. Within 2−6 m, the structural parameter CH_2/CH_3 fluctuates, and when it is greater than 6 m, CH_2/CH_3 tends to be stable. Overall, the aliphatic structural parameters of demineralized coal are lower than those of raw coal, which indicates that the hydrocarbon chain length of raw coal is longer than that of demineralized coal. The length of the aliphatic chain decreases and the aromaticity increases after demineralization, indicating that the length and number of cross-linked branches at the edge of the aromatic layer in coal are reduced, which is conducive to the ordering of the two-dimensional structure in coal. After graphitization, the aliphatic CH_2/CH_3 of coal-based graphite decreased significantly and tended to be similar, indicating that graphitization eliminated a large number of aliphatic side chains and stacked the graphite into a three-dimensional ordered structure. However, this effect obviously did not reach 100%, which was also confirmed by the aromatic structure parameters f_{ar}^H, I, and DOC. The CH_2/CH_3 of coal-based graphene oxide and coal-based graphene is slightly higher than that of coal-based graphite, which may be because of strong oxidants and reductants on −CH_3 in the process of oxidation and reduction, which makes CH_2/CH_3 larger. This does not indicate the growth of aliphatic chains.
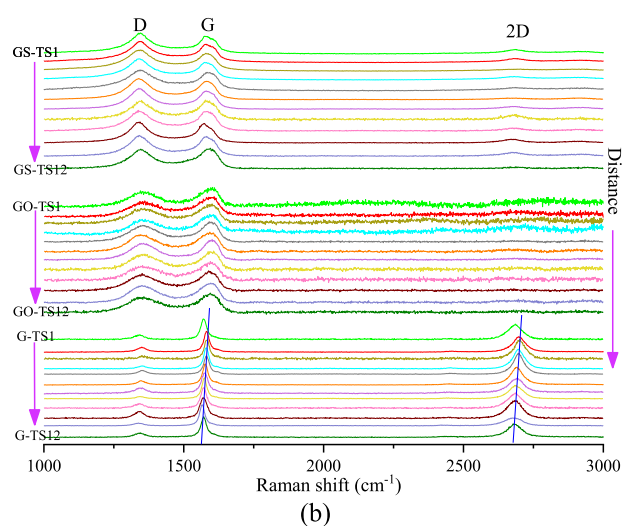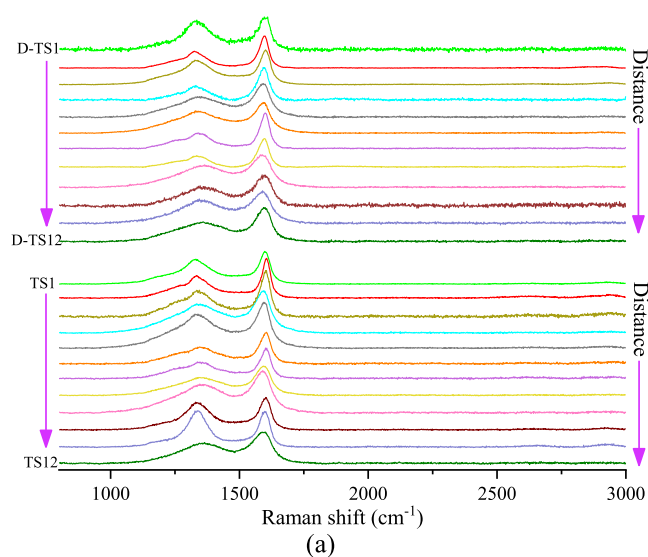
Figure 4e shows the correlation of the parameter "C" of the ratio of C=O functional groups to C=O and C=C functional groups of samples and products at different distances from the dike. "C" is used to indicate the maturity of the coal and the degree of oxidation. In all samples and products, "C" has a jump within 1 m, which indicates that TS1 in direct contact with the dike has more oxygen-containing functional groups. Within 0.1−6 m (TS1-TS8), the "C" value of the bulk of samples and products increases with distance from the dike, indicating that the maturity gradually decreases and the oxygen-containing functional groups increase. When it is greater than 6 m (TS9-TS12), the "C" value of the original coal tends to be stable, which is similar to CH_2/CH_3. Due to the destruction of C=O by strong acids in demineralization, the "C" value of demineralized coal is lower than that of raw coal. Therefore, there are fewer oxygen-containing functional groups in demineralized coal. After graphitization, the "C" value decreases significantly, indicating that during the graphitization process, C=O was broken, and a large number of aromatic layers and graphite microcrystals were generated, resulting in an increase in C=C. After the coal-based graphite was intercalated with a strong oxidant, the sp^2 hybrid crystalline carbon structure in the coal-based graphite structure was destroyed, and a large number of oxygen-containing functional groups were introduced on the surface to form graphene oxide (see Figure 2b), resulting in a sharp increase in the "C" value. Various functional groups introduced by intercalation increase the interlayer spacing of aromatic layers and reduce the intermolecular force, which provides conditions for the stripping and reduction of coal-based graphene. Compared with the corresponding coal-based graphite, the coal-based graphene oxide surface obviously contains a variety of oxygen-containing groups, mainly including C=O, C−O, and O−H. After reduction, the peaks of various oxygen functional groups in the range of 1000−2000 cm^{-1} decreased significantly, indicating that the oxygen-containing functional

groups were effectively removed, and the "C" value decreased significantly.[67] However, it is found from the "C" value of coal-based graphene that coal-based graphene oxide is not completely reduced, mainly because the large number of ethers and/or epoxides (1000−1280 cm^{-1}) introduced in the oxidation process will form pyrans and furans, which are difficult to reduce and completely remove. In addition, there is almost no difference in the typical peaks of all coal-based graphene, indicating that the effect of redox processes on functional group elimination, free radical dissociation, and bond formation of altered coal-based products and unaltered coal-based products is similar.

3.3. Raman Results. Raman spectroscopy plays an important role in studying the structural defects of carbon materials, providing information on defects, stacking, and disorder of graphite and graphite series products. The common Raman peaks of carbon materials are D_1 peak (~1350 cm^{-1}), G peak (~1580 cm^{-1}), 2D peak (~2700 cm^{-1}), and D + G peak (2940 cm^{-1})[68−70] (Figure 5). The G peak is caused by the stretching vibration of the sp^2 bond in the hexagonal aromatic molecules of single crystal graphite; The D_1 peak represents the lattice defects and edge disorder of graphite-type carbon materials; The 2D peak represents the interlayer stacking mode of carbon atoms; The D + G peak is caused by the combination of the D and G peaks. This experiment conducted Raman testing on the sample in the wavenumber range of 1000−3000 cm^{-1}. Using the area ratio of D_1 peak to G peak (A_{D1}/A_G) to characterize the degree of disorder in the structure of carbon materials, the larger the value, the higher the degree of disorder in the samples and products. It is worth noting that for Figure 5b, the G peaks of G-TS1 to G-TS12 have become exceptionally sharp and have formed distinct 2D peaks. The formation of the G peak is related to the condensation and ordered arrangement of aromatic layers in coal, while the 2D peak is sensitive to the stacking order of graphene sheets along the c-axis, indicating that all coal samples have been transformed into graphite after graphitization treatment. Moreover, the coal sample attached to the intrusion is bound to be contaminated and damaged by the intrusion,[22,29,41] except for the damaged TS1, as the distance from the intrusion becomes closer, the G and 2D peaks shift significantly to the right, indicating that the closer the thermally altered distance, the more obvious the graphitization characteristics.

To describe the structural characteristics of coal more accurately, a detailed curve fitting analysis was carried out on the first-order Raman spectrum (Figure 6, taking the TS6 sample as an example). According to previous studies, the Raman shift peak position assignments were summarized (see Table 3).[33,34,40,71,72] According to the peak position and relative area intensity obtained by fitting the peak position, the macromolecular structural information on the samples and products (see Appendices A3 and A4) can be obtained. From Appendix A4, it can be found that except for GS-TS1 closest to the intrusion and GS-TS12 farthest from the intrusion, the I_{2D}/I_G distribution of other products is between 0.25 and 0.42, which are multilayer graphene. The three most commonly used parameters are $fwhm_G$, A_{D1}/A_G, and G-D_1 to measure the degree of carbon atoms in samples and products, and the relationship between the three indices and distance from the dike is shown in Figure 7.[33,40,73−75]

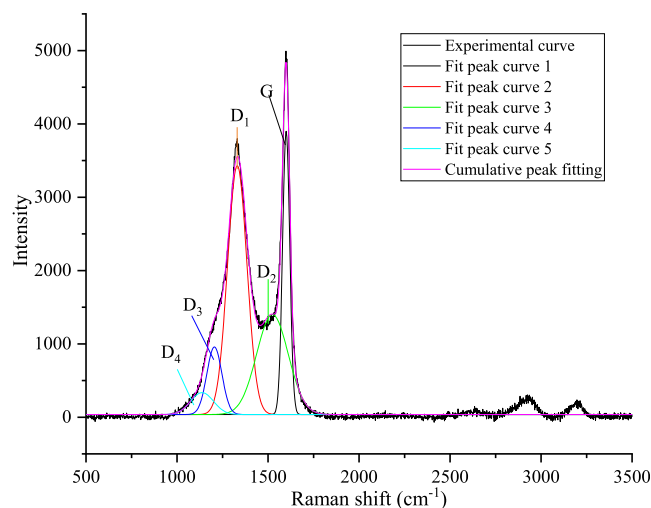From Figure 7a, we can see the relationship between the $fwhm_G$ and distance; a smaller $fwhm_G$ value usually indicates a larger aromatic lamellar structure in materials. Overall, the $fwhm_G$ value of coal-based graphite is the smallest, and the fluctuation range is also the smallest, which is caused by

Figure 5. Raman spectra of coal samples and coal-based products: (a) raw coals and demineralized coal; (b) coal-based graphite, coal-based graphite oxide, and coal-based graphene.

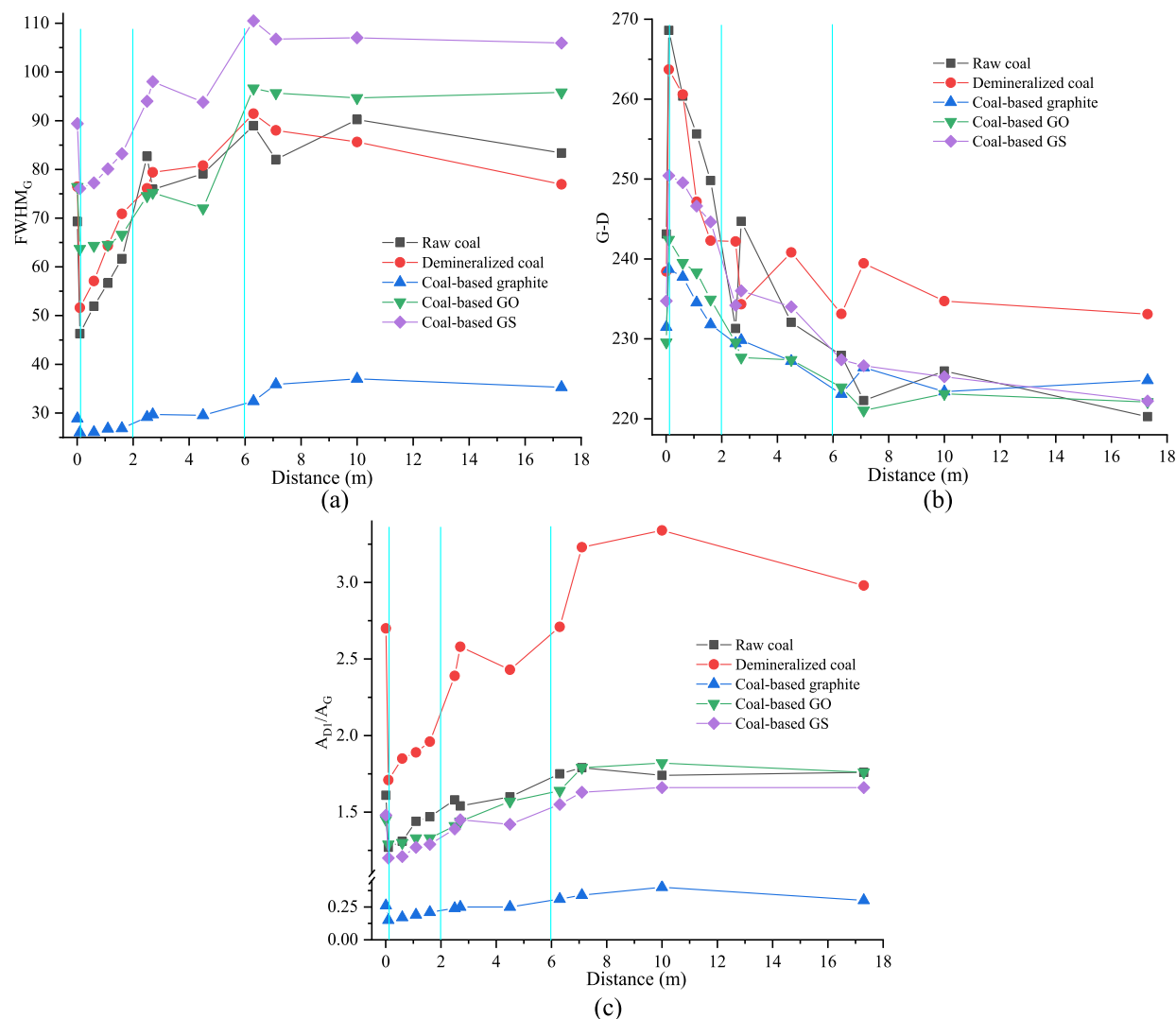**Figure 6.** Curve-fitting Raman spectrum of sample TS6.

Table 3. Raman Spectrum Band/Peak Assignment in Coals (Summary From Refs 33,40,73−75)

band name	position (cm^{-1})	functional groups	bond type
D_1	1350	D1 1350 C−C between aromatic rings and aromatics with not <6 rings	SP^2
D_2	1540	amorphous carbon structures; aromatics with 3−5 rings;	SP^2
D_3	1230	aryl-alkyl ether; para-aromatics	SP^2, $SP^{3'}$
D_4	1185	Caromatic - Calkyl; aromatic (aliphatic) ethers; C−C on hydroaromatic rings;hexagonal diamond carbon sp^3; C−H onaromatic rings	SP^2, $SP^{3'}$
G	1590	graphite E_{2g}^2; aromatic ring quadrantbreathing; alkene C═C	SP^2

series products, which is more obvious in the Raman diagram of coal-based graphite (Figure 5b). Figure 7b shows that for both the coal samples and coal-based series products, the G-D value shows abnormal thermally altered characteristics within 0.1 m and maintains the leveling characteristics of the original coal over 6 m. In the range of 0.1−6 m, the G-D values of the bulk of samples and products gradually decrease with the increase of reflectivity. It is worth noting that the variation characteristics of the G-D values of samples and products within 2−6 m are different from those of the reflectance, proximate analysis, and ultimate analysis. Therefore, combined with the FTIR parameters and fwhm$_G$ value, the 2−6 m region can be regarded as a thermally altered transition zone. The G-D of the coal samples and their carbon materials at a distance over six meters tend to stabilize and remain almost consistent, indicating that they are no longer affected by the intrusion. Therefore, it is speculated that the original coal zone is located at a distance of six meters away from the intrusion.

The A_{D1}/A_G value is an important index to measure the degree of order of carbon materials. Generally, the smaller the A_{D1}/A_G value is, the better the degree of order of carbonaceous materials. Figure 7c shows that the A_{D1}/A_G value of demineralized coal is very high, which is caused by the destruction of the order of the coal structure after the removal of minerals. After graphitization, the A_{D1}/A_G value of coal-based graphite decreases significantly, and the fluctuation range is very small, indicating that graphitization can make coal samples in different thermally altered zones obtain almost consistent

the growth of aromatic layers and the formation of graphite microcrystals during graphitization. However, the fwhm$_G$ value of coal-based graphene is the largest, which is caused by the stripping of aromatic layers of the coal-based graphite stack in the oxidation−reduction. Within 0.1 m, the fwhm$_G$ values of both samples and products decrease from TS1 and reach minimum values at TS2, which shows that the aromatic lamellar structure of TS1 series products attached to the dike has been destroyed by magma, and the degree of aromatic order of TS2 series products is the best. Within 0.1−2 m, the value of the fwhm$_G$ increases significantly with decreasing reflectance, indicating that the aromatic structure gradually decreases, which is consistent with the aromatic parameters of FTIR, and this is a typical thermally altered feature. Within 2−6 m, the fwhm$_G$ value fluctuates after rising, with an obvious transition trend, and after 6 m, the fwhm$_G$ value tends to stabilize.

The relationship between G-D$_1$ and distance is shown in Figure 7b. It can be seen from the parameters Appendices A3 and A4 that with the increase in reflectance (excluding TS1 in the abnormal thermally altered zone), there is a right shift trend in the position of the G peak in both coal samples and coal-based

Figure 7. Comparison of the variation in Raman parameters between coal samples and coal-based products with different distances from the dike: (a) fwhm$_G$, full width at half maxima of G peak; (b) G-D, Peak position difference between peak G and peak D; (c) A_{D1}/A_G, ratio of D peak area to G peak area.

ordering. It can also be seen from Figure 7c that the A_{D1}/A_G value of coal-based graphene oxide after oxidative intercalation increases and the degree of order decreases. However, after reduction, the A_{D1}/A_G value of coal-based graphene decreases, which is related to the removal of oxygen-containing functional groups, confirming the change trend of the 'C' of the FTIR parameter after oxidation and reduction.

3.4. Yield Analysis of Coal-Based Graphene. The steps of preparation process of coal-based graphene can be simply divided into several stages: raw coal, demineralized coal, artificial graphite, graphite oxide solution, graphene oxide solution, and solid graphene. The process from coal-based graphite to solid coal-based graphene is through oxidation, ultrasound, centrifugation, reduction, and other processes. The experimental operation is cumbersome, which easily causes sample loss. Therefore, the final graphene yield is shown in the table.

The coal-based graphene yield based on coal-based graphite is recorded as W_G, the coal-based graphene yield based on raw coal is recorded as W_C, the weight of raw coal used for demineralization is recorded as M_C, the weight of demineralized coal sample obtained after demineralization is recorded as M_D, the demineralization yield is recorded as D, where $D = M_D/M_C$ the weight of

demineralized coal sample for graphitization is recorded as M_{D1}, the weight of coal-based graphite obtained after graphitization is recorded as M_G, the coal-based graphite yield is recorded as G, where $G = M_G/M_{D1}$, the weight of the artificial graphite used to prepare graphene is recorded as M_{G1}, and the weight of the obtained graphene is recorded as M_{GS}. According to the preparation process, the yield formula of graphene from raw coal in this study is as follows:

$$W_c = M_{GS} \cdot \frac{M_G}{M_{G1}} \cdot \frac{M_D}{M_{D1}} \cdot \frac{1}{M_C} = W_G \cdot G \cdot D$$

$$W_G = \frac{M_{GS}}{M_{G1}} \times 100\%$$

Through calculation, the yield of graphene is shown in Table 4. According to Table 4, the highest yield of graphene based on raw coal of the sample is 6.23% of TS2, and the yield of graphene of other samples is between 3.43 and 5.88%. According to the distance from the dike, the yield of graphene can be divided into four stages. For TS1 with an abnormally altered zone (within 0.1 m), the yield of graphene is 4.87%; TS2-TS5 in the normally

Table 4. Yield of Graphene from Raw Coal

sample	D	G	M_{G1}/g	M_{GS}/g	W_G/%	W_C/%
TS1	0.89	0.80	2.0019	0.1369	6.84	4.87
TS2	0.93	0.87	2.0051	0.1556	7.76	6.23
TS3	0.91	0.84	2.006	0.1493	7.44	5.67
TS4	0.91	0.82	2.0107	0.1465	7.29	5.42
TS5	0.92	0.80	2.0093	0.1420	7.07	5.18
TS6	0.92	0.70	2.0101	0.1381	6.87	4.43
TS7	0.92	0.69	2.0015	0.1344	6.71	4.26
TS8	0.91	0.66	2.0057	0.1228	6.12	3.69
TS9	0.89	0.66	2.0052	0.1230	6.13	3.61
TS10	0.92	0.65	2.0024	0.1227	6.13	3.64
TS11	0.92	0.65	2.0065	0.1220	6.08	3.62
TS12	0.91	0.66	2.0179	0.1225	6.07	3.62
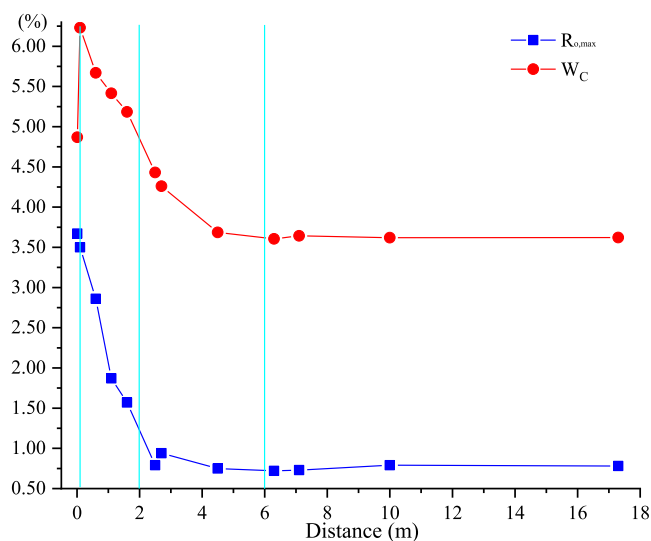
Figure 8. Trend of reflectance and graphene yield of raw coal with the distance from the dike.

Figure 9. Division of the thermally altered zone and distribution of the yield and quality of coal-based graphene in zones.

altered zone (0.1−2 m) has a yield of 5.18−6.23%; for TS6-TS8 in the transition zone (2−6 m), the yield is in the range of 3.69−4.43%; and for TS9-TS12 (over 6 m) of the original coal zone, and the yield is in the range of 3.61−3.64%.

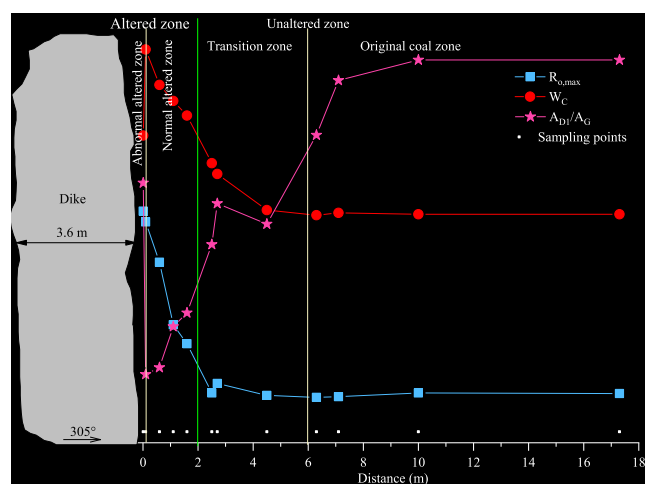It can be seen from the Figure 8 that with increasing distance from the dike, the yield of coal-based graphene and the reflectance of coal show a similar trend, first decreasing and then stabilizing. However, the difference is that there is an abnormal jump in the graphene yield at 0.1 m, and the yield of coal-based graphene shows a decreasing trend within 2−6 m, while the reflectance tends to be stable in this distance range.

3.5. Division of the Thermally Altered Zone. Combining A_{D1}/A_G, which indicates the quality parameter of coal-based graphene (the higher the A_{D1}/A_G ratio, the lower the order of samples and products), with the yield value (W_C), can better divide the thermally altered zone of this study. Figure 9 shows that the sampling area can be divided into an altered zone and an unaltered zone with a boundary of 2 m according to the reflectance proximate analysis and ultimate analysis of coal. According to the FTIR and Raman parameters of coal and coal-based products, the altered zone is divided into an abnormally altered zone and a normally altered zone with a boundary of 0.1 m; The nonthermal zone is divided into a transition zone and an original coal zone with a boundary of 6 m. The abnormally altered zone (within 0.1 m), although the reflectance of coal

sample in this zone is the highest, due to the destruction of magmatic heat and exogenous materials, the aromaticity and structural parameters of coal sample and products are abnormal; normal altered zone (0.1−2.0 m), the aromaticity and order of structure of samples and products in this zone are better than those in other bands, and the structural parameters of the bulk of samples and products increase or decrease with reflectance, which is a typical thermal altered feature; transition zone (2.0−6.0 m), although the reflectance of the samples in this zone is the same as that of the original coal in this study area, the aromatic parameters, aliphatic parameters and degree of order of samples and products in this zone are between normal altered coal and original coal and fluctuate; original coal zone (more than 6.0 m), almost all parameters of samples and products tend to be stable in this band.

It can also be seen from Figures 8 and 9 that the coal-based graphene prepared from the samples of the normal altered zone is the best in both yield and quality, and yield and quality are positively correlated with reflectance. Although TS1 in the abnormally altered zone has a high yield of graphene, the quality of coal-based graphene prepared by it is not very good due to the destruction of magmatic heat and the pollution of exogenous substances. The yield and quality of coal-based graphene prepared from the samples in the transition zone are between those of the normal altered zone and the original coal zone. The yield and quality of coal-based graphene from original coal are the worst, which is caused by its coal quality and coal structure attributes. Therefore, for the yield of coal-based graphene, the order of the zones from highest to lowest is as follows: the normal altered zone, the abnormally altered zone, transition zone, and the original coal zone; for the quality of coal-based graphene, the order of the zones from highest to lowest is as follows: the normal altered zone, transition zone, abnormally altered zone, and original coal zone. Except for the abnormally altered zone, magmatic contact metamorphism is beneficial to the coal structure as well as the yield and quality of coal-based graphitic products, and coals in the normal altered zone are the ideal materials for coal-based graphene.

4. CONCLUSIONS

Through FTIR and Raman spectral analysis, the structural parameters f_{ar}^H, I, DOC, CH_2/CH_3, 'C', G-D_1 and A_{D1}/A_G of Tashan thermally altered coal and coal-based graphitic materials

with different distances from the dike, and the following conclusions were drawn:

The aromaticity and degree of order of Tashan thermally altered coal increase with increasing of reflectance. Due to the cutting effect of strong acids on aliphatic chains, the aromaticity of coal slightly increases, and the aliphatic parameters slightly increase after demineralization. However, demineralization cannot improve the degree of order of the coal structure. In contrast, the removal of minerals in coal destroys the aromatic structure, resulting in a significant reduction in the degree of order, with the most obvious change in the A_{D1}/A_G value.

Graphitization can eliminate a large number of aliphatic chains in the sample, significantly improve the aromaticity parameters f_{ar}^H and I, and significantly reduce the degree of oxidation degree "C". The degree of order of the samples after graphitization is greatly improved and tends to be similar. Redox reaction will reduce the aromatic parameters of the products, the degree of oxidation after oxidation is significantly increased, and the ether functional groups brought by the oxidation intercalation are difficult to reduce and remove. The degree of order of coal-based graphene from Tashan thermally altered coal, is positively correlated with the original structural parameters of the raw coal.

Through the analysis of the evolution trend of FTIR and Raman parameters of coal samples and products, the Tashan thermally altered area can be divided into four zones from near to far from the dike: the abnormally altered zone, normal altered zone, transition zone, and original coal zone. The evolution of structural parameters of thermally altered coal and coal-based

graphitic products is from jumping to gradual change, then to fluctuation and finally tends to be stable. The variation trend of the graphene yield and quality with the distance from the dike basically conforms to the characteristics of the four zones. Magmatic contact metamorphism can improve the original structure of coal and improve the yield and quality of coal-based graphene. For the coal resources in the thermally altered zone, the coals in the normal altered zone are the ideal raw material sources of coal-based carbon materials.

The study of using the structural parameters of coal and coal-based carbon materials to divide the thermally altered zones is still in the exploratory stage. Multiple comprehensive characterization parameter indicators should be applied in future thermally altered zones division work, such as XRD, XPS, NMR, AFM, TEM, STM, etc. This study could provide a template for the division of other thermally altered regions in the future. Differences in the scale, temperature, and duration of intrusions in other thermally altered regions may result in different division distances, but the types of zones should be consistent. In this study, coal samples from the normal altered zone are ideal raw materials for carbon materials, which also provides reference for other fields. However, for natural thermally altered regions, we cannot consider the extension of normal altered zones. However, we can consider large-scale, high-temperature, and long-acting intrusion dikes, which can cause larger thermally altered halos and theoretically, more normal altered zones.

■ APPENDIX A

Table A1. Structural Parameters of Raw Coal and Demineralized Coal from FTIR Spectra

sample	distance (m)	$R_{o,max}$ (%)	f_{ar}^H	f_{ar}^C	I	CH_2/CH_3	DOC	'C'
TS1	0.01	3.67	0.58	0.97	3.24	0.54	1.18	0.17
TS2	0.1	3.50	0.71	0.96	4.32	0.59	1.34	0.11
TS3	0.6	2.86	0.67	0.94	4.19	0.61	1.23	0.12
TS4	1.1	1.87	0.61	0.90	3.46	0.71	1.15	0.15
TS5	1.6	1.57	0.61	0.83	2.60	0.92	0.99	0.19
TS6	2.5	0.79	0.42	0.79	1.12	1.86	0.65	0.28
TS7	2.7	0.94	0.44	0.79	1.23	1.90	0.58	0.26
TS8	4.5	0.75	0.40	0.76	1.06	1.93	0.57	0.26
TS9	6.3	0.72	0.28	0.71	0.57	3.71	0.32	0.35
TS10	7.1	0.73	0.24	0.72	0.67	4.66	0.33	0.34
TS11	10.0	0.79	0.27	0.70	0.52	4.59	0.40	0.37
TS12	17.3	0.78	0.23	0.68	0.53	3.64	0.39	0.35
D-TS1	0.01		0.66		4.94	0.18	1.33	0.15
D-TS2	0.1		0.87		5.01	0.20	1.39	0.10
D-TS3	0.6		0.75		4.67	0.20	1.30	0.10
D-TS4	1.1		0.63		4.11	0.27	1.25	0.11
D-TS5	1.6		0.62		4.03	0.33	1.14	0.14
D-TS6	2.5		0.50		2.91	0.82	0.71	0.21
D-TS7	2.7		0.52		3.33	1.02	0.58	0.24
D-TS8	4.5		0.49		2.65	0.79	0.63	0.19
D-TS9	6.3		0.43		0.93	1.67	0.44	0.26
D-TS10	7.1		0.41		1.13	1.80	0.38	0.29
D-TS11	10.0		0.44		1.07	1.76	0.44	0.30
D-TS12	17.3		0.43		0.90	1.94	0.39	0.25

Table A2. Structural Parameters of Coal-Based Graphite, Coal-Based Graphene Oxide, and Coal-Based Graphene from FTIR Spectra

sample	distance (m)	f_{ar}^H	f_{ar}^C	I	CH_2/CH_3	DOC	'C'
G-TS1	0.01	0.97		41.22	0.01	0.75	0.04
G-TS2	0.1	0.98		55.26	0.01	0.97	0.01
G-TS3	0.6	0.99		45.69	0.03	0.92	0.02
G-TS4	1.1	0.99		49.10	0.01	0.95	0.02
G-TS5	1.6	0.98		44.72	0.02	0.85	0.03
G-TS6	2.5	0.96		29.80	0.02	0.77	0.07
G-TS7	2.7	0.97		27.09	0.06	0.80	0.05
G-TS8	4.5	0.97		32.44	0.01	0.82	0.08
G-TS9	6.3	0.95		20.45	0.08	0.72	0.07
G-TS10	7.1	0.97		18.65	0.10	0.66	0.12
G-TS11	10.0	0.95		19.77	0.02	0.75	0.12
G-TS12	17.3	0.94		21.34	0.05	0.69	0.11
GO-TS1	0.01	0.96		57.17	0.14	0.78	0.56
GO-TS2	0.1	0.99		66.92	0.10	1.04	0.45
GO-TS3	0.6	0.95		60.22	0.11	0.83	0.53
GO-TS4	1.1	0.98		62.91	0.11	0.90	0.49
GO-TS5	1.6	0.98		53.48	0.09	0.67	0.47
GO-TS6	2.5	0.94		40.09	0.13	0.95	0.69
GO-TS7	2.7	0.97		36.70	0.09	0.85	0.61
GO-TS8	4.5	0.95		45.41	0.13	0.66	0.65
GO-TS9	6.3	0.96		28.74	0.11	0.79	0.71
GO-TS10	7.1	0.97		25.05	0.15	0.70	0.68
GO-TS11	10.0	0.95		25.83	0.12	0.64	0.65
GO-TS12	17.3	0.94		29.04	0.13	0.68	0.64
GS-TS1	0.01	0.97		60.04	0.31	0.93	0.12
GS-TS2	0.1	0.99		65.23	0.26	1.11	0.10
GS-TS3	0.6	0.96		61.97	0.21	1.03	0.15
GS-TS4	1.1	0.98		52.69	0.35	0.95	0.14
GS-TS5	1.6	0.95		54.45	0.44	1.15	0.14
GS-TS6	2.5	0.95		42.90	0.30	0.88	0.16
GS-TS7	2.7	0.94		41.76	0.29	0.79	0.15
GS-TS8	4.5	0.90		45.77	0.56	0.83	0.20
GS-TS9	6.3	0.93		29.01	0.41	0.61	0.18
GS-TS10	7.1	0.96		31.47	0.36	0.69	0.19
GS-TS11	10.0	0.89		32.70	0.29	0.73	0.16
GS-TS12	17.3	0.94		30.05	0.35	0.70	0.15

Table A3. Structural Parameters of Raw Coal and Demineralized Coal from Raman Spectra

sample	distance (m)	D1 (cm^{-1}) position	D1 (cm^{-1}) fwhm	G (cm^{-1}) position	G (cm^{-1}) fwhm	A_{D1}/A_G	G–D1
TS1	0.01	1347.44	186.10	1590.56	69.28	1.61	243.12
TS2	0.1	1330.92	125.26	1599.52	46.30	1.27	268.60
TS3	0.6	1337.86	90.86	1598.23	51.92	1.31	260.37
TS4	1.1	1339.81	170.97	1595.45	56.66	1.44	255.64
TS5	1.6	1343.13	181.79	1592.94	61.67	1.47	249.81
TS6	2.5	1359.45	216.89	1590.75	82.69	1.58	231.30
TS7	2.7	1348.95	197.74	1593.65	75.88	1.54	244.70
TS8	4.5	1359.97	136.76	1592.03	79.13	1.60	232.06
TS9	6.3	1365.40	177.34	1593.33	88.97	1.75	227.93
TS10	7.1	1373.23	169.98	1595.51	82.05	179	222.28
TS11	10.0	1368.25	150.99	1594.23	90.25	1.74	225.98
TS12	17.3	1371.21	140.51	1591.47	83.37	1.76	220.26
D-TS1	0.01	1353.31	178.59	1591.75	76.46	2.70	238.44
D-TS2	0.1	1335.43	122.59	1599.13	51.62	1.71	263.7
D-TS3	0.6	1340.48	117.82	1601.06	57.11	1.85	260.58
D-TS4	1.1	1349.87	165.90	1597.04	64.33	1.89	247.17
D-TS5	1.6	1346.57	139.75	1588.87	70.89	1.96	242.30

Table A3. continued

sample	distance (m)	D1 (cm⁻¹) position	D1 (cm⁻¹) fwhm	G (cm⁻¹) position	G (cm⁻¹) fwhm	A_{D1}/A_G	G-D1
D-TS6	2.5	1354.11	172.19	1596.30	76.10	2.39	242.19
D-TS7	2.7	1359.52	215.46	1593.86	79.40	2.58	234.34
D-TS8	4.5	1358.30	165.32	1599.12	80.79	2.43	240.82
D-TS9	6.3	1365.49	160.67	1598.62	91.44	2.71	233.13
D-TS10	7.1	1361.26	197.49	1600.71	88.03	3.23	239.45
D-TS11	10.0	1362.54	180.59	1597.27	85.63	3.34	234.73
D-TS12	17.3	1370.81	170.03	1603.9	76.95	2.98	233.09

Table A4. Structural Parameters of Coal-Based Graphite, Coal-Based Graphene Oxide, and Coal-Based Graphene from Raman Spectra

sample	distance (m)	D1 (cm⁻¹) position	D1 (cm⁻¹) fwhm	G (cm⁻¹) position	G (cm⁻¹) fwhm	A_{D1}/A_G	G-D1	I_{2D}/I_G
G-TS1	0.01	1350.06	38.48	1581.54	28.87	0.26	231.48	
G-TS2	0.1	1347.89	38.73	1586.62	26.02	0.15	238.73	
G-TS3	0.6	1348.79	40.19	1585.54	26.06	0.17	237.75	
G-TS4	1.1	1349.27	38.01	1583.81	26.77	0.19	234.54	
G-TS5	1.6	1348.30	46.81	1580.10	26.85	0.21	231.80	
G-TS6	2.5	1350.29	41.04	1579.72	29.15	0.24	229.43	
G-TS7	2.7	1347.24	44.53	1577.08	29.70	0.25	229.84	
G-TS8	4.5	1350.86	43.14	1578.07	29.54	0.25	227.21	
G-TS9	6.3	1351.65	44.98	1574.74	32.41	0.31	223.09	
G-TS10	7.1	1348.19	47.58	1573.60	35.87	0.34	226.41	
G-TS11	10.0	1349.68	46.56	1572.08	37.02	0.40	223.40	
G-TS12	17.3	1350.38	45.94	1575.19	35.28	0.30	224.81	
GO-TS1	0.01	1360.26	159.87	1589.83	76.43	1.45	229.57	
GO-TS2	0.1	1355.46	144.88	1597.87	63.71	1.29	242.41	
GO-TS3	0.6	1358.45	151.96	1597.97	64.33	1.30	239.52	
GO-TS4	1.1	1358.30	139.83	1596.62	64.53	1.33	238.32	
GO-TS5	1.6	1360.61	138.48	1595.54	66.60	1.33	234.93	
GO-TS6	2.5	1361.42	137.03	1590.97	74.55	1.41	229.55	
GO-TS7	2.7	1360.78	141.03	1588.45	75.21	1.44	227.67	
GO-TS8	4.5	1360.14	140.75	1585.52	72.01	1.57	227.38	
GO-TS9	6.3	1361.37	139.07	1585.31	96.63	1.64	223.94	
GO-TS10	7.1	1364.90	136.55	1585.95	95.67	1.79	221.05	
GO-TS11	10.0	1361.57	126.67	1584.69	94.68	1.82	223.12	
GO-TS12	17.3	1360.69	138.28	1582.80	95.82	1.76	222.11	
GS-TS1	0.01	1345.78	150.60	1580.53	89.40	1.48	234.75	0.19
GS-TS2	0.1	1342.93	142.59	1593.36	76.09	1.20	250.43	0.35
GS-TS3	0.6	1342.94	132.18	1592.49	77.24	1.21	249.55	0.42
GS-TS4	1.1	1343.72	135.84	1590.34	80.09	1.27	246.62	0.37
GS-TS5	1.6	1345.09	139.84	1589.72	83.23	1.29	244.63	0.33
GS-TS6	2.5	1346.02	133.63	1580.22	94.00	1.39	234.2	0.30
GS-TS7	2.7	1346.53	154.58	1582.54	98.02	1.45	236.01	0.30
GS-TS8	4.5	1347.69	129.52	1581.70	93.81	1.42	234.01	0.28
GS-TS9	6.3	1348.68	144.63	1576.07	110.51	1.55	227.39	0.27
GS-TS10	7.1	1348.05	139.24	1574.69	106.75	1.63	226.64	0.27
GS-TS11	10.0	1347.81	142.71	1573.06	107.03	1.66	225.25	0.25
GS-TS12	17.3	1350.30	145.46	1572.53	105.94	1.66	222.23	0.15

■ AUTHOR INFORMATION

Corresponding Author

Yuegang Tang − *College of Geoscience and Surveying Engineering, China University of Mining and Technology (Beijing), Beijing 100083, China;* ◎ orcid.org/0000-0002-2260-6113; Email: tyg@vip.163.com, tyg@cumtb.edu.cn

Authors

Ruiqing Li − *College of Geoscience and Surveying Engineering, China University of Mining and Technology (Beijing), Beijing 100083, China*

Xiaoxia Song − *Department of Geoscience and Engineering, Taiyuan University of Technology, Taiyuan 030024, China*

Shaoqing Wang − *College of Geoscience and Surveying Engineering, China University of Mining and Technology (Beijing), Beijing 100083, China;* ⊙ orcid.org/0000-0001-5158-7751

Qili Che − *College of Geoscience and Surveying Engineering, China University of Mining and Technology (Beijing), Beijing 100083, China*

Cong Chen − *College of Geoscience and Surveying Engineering, China University of Mining and Technology (Beijing), Beijing 100083, China*

Complete contact information is available at:
https://pubs.acs.org/10.1021/acsomega.4c01845

Author Contributions

■ REFERENCES

(1) Lee, C.; Wei, X.; Jeffrey, W.; James, H. Measurement of the Elastic Properties and Intrinsic Strength of Monolayer Graphene. *Science* **2008**, *321*, 385−388.

(2) Reina, A.; Jia, X.; Ho, J.; Nezich, D.; Son, H.; Bulovic, V.; Dresselhaus, M. S.; Kong, J. Large Area, Few-layer Graphene Films on Arbitrary Substrates by Chemical Vapor Deposition. *Nano Lett.* **2009**, *9*, 30−35.

(3) Liang, M.; Luo, B.; Zhi, L. Application of Graphene and Graphene-Based Materials in Clean Energy-Related Devices. *Int. J. Energ Res.* **2009**, *33*, 1161−1170.

(4) Li, R.; Tang, Y.; Che, Q.; Huan, X.; Ma, P.; Luo, P.; Mao, X. Study on the Microstructure of the Symbiosis of Coal-Based Graphene and Coal-Based Graphene Quantum Dots: Preparation and Characterization. *Nanotechnology* **2022**, *33* (45), No. 455702.

(5) Ye, R.; Xiang, C.; Lin, J.; Peng, Z.; Huang, K.; Yan, Z.; Cook, N. P.; Samuel, E. L. G.; Hwang, C.-C.; Ruan, G. D.; Ceriotti, G.; Raji, A. O.; Marti, A. A.; Tour, J. M. Coal as An Abundant Source of Graphene Quantum Dots. *Nat. Commun.* **2013**, *4*, 2943.

(6) Huan, X.; Tang, Y.; Xu, J.; Lan, C.; Wang, S. Structural Characterization of Graphenic Material Prepared from Anthracites of Different Characteristics: A Comparative Analysis. *Fuel Process. Technol.* **2019**, *183*, 8−18.

(7) Li, R.; Tang, Y.; Che, Q.; Ma, P.; Luo, P.; Lu, X.; Dong, M. Effects of Coal Rank and Macerals on The Structure Characteristics of Coal-Based Graphene Materials from Anthracite in Qinshui Coalfield. *Minerals.* **2022**, *12*, 588.

(8) Wang, L.; Zhang, H.; Li, Y. On The Difference of Characterization and Supercapacitive Performance of Graphene Nanosheets from Precursors of Inertinite- And Vitrinite-Rich Coal. *J. Alloys Compd.* **2020**, *815*, No. 152502.

(9) Lan, C.; Tang, Y.; Huan, X.; Che, Q. Effects of Minerals in Anthracite on The Formation of Coal-Based Graphene. *ChemistrySelect* **2019**, *19*, 5937−5944.

(10) Stach, E.; Mackowsky, M. T.; Teichmüller, M. *Stach's Textbook of Coal Petrology*; Gebrüder Borntraeger: Berlin Stuttgart, 1982.

(11) Bustin, R. M.; Rouzaud, J. N.; Ross, J. V. Natural Graphitization of Anthracite: Experimental Considerations. *Carbon* **1995**, *33*, 679−691.

(12) Mhlwazi, S.; Clifford, C. B.; Schobert, H. H. Characterization of Graphitic Materials Prepared from Different Rank Pennsylvania Anthracites. *Fuel* **2012**, *114*, 244−250.

(13) Zhang, S.; Song, B.; Cao, C.; Zhang, H.; Liu, Q.; Li, K.; Teppen, B. J. Structural Evolution of High-Rank Coals During Coalification and Graphitization: X-Ray Diffraction, Raman Spectroscopy, High-Resolution Transmission Electron Microscopy, And Reactive Force Field Molecular Dynamics Simulation Study. *Energ Fuel.* **2021**, *35*, 2087−2097.

(14) Stewart, A. K.; Massey, M.; Padgett, P. L.; Rimmer, S. M.; Hower, J. C. Influence of A Basic Intrusion on The Vitrinite Reflectance and Chemistry of The Springfield (No. 5) Coal, Harrisburg, Illinois. *Int. J. Coal Geol.* **2005**, *63*, 58−67.

(15) Dai, S.; Ren, D. Effects of Magmatic Intrusion on Mineralogy and Geochemistry of Coals from The Fengfeng-Handan Coalfield, Hebei, China. *Energ Fuel.* **2007**, *21*, 1663−1673.

(16) Mastalerz, M.; Drobniak, A.; Schimmelmann, A. Changes in Optical Properties, Chemistry, And Micropore and Mesopore Characteristics of Bituminous Coal at The Contact with Dikes in The Illinois Basin. *Int. J. Coal Geol.* **2009**, *77*, 310−319.

(17) Goodarzi, F.; Murchison, D. G. Effect of Prolonged Heating on the Optical Properties of Vitrinite. *Fuel.* **1977**, *56*, 89−96.

(18) Goodarzi, F.; Murchison, D. G. Influence of Heating-Rate Variation on the Anisotropy of Carbonized Vitrinites. *Fuel* **1978**, *57*, 273−284.

(19) Shi, Q.; Qin, B.; Liang, H.; Gao, Y.; Bi, Q.; Qu, B. Effects of Igneous Intrusions on The Structure and Spontaneous Combustion Propensity of Coal: A Case Study of Bituminous Coal in Daxing Mine. *China. Fuel.* **2018**, *216*, 181−189.

(20) Matlala, I. V.; Moroeng, O. M.; Wagner, N. J. Macromolecular Structural Changes in Contact Metamorphosed Inertinite-Rich Coals from The No.2 Seam, Witbank Coalfield (South Africa): Insights from Petrography, NMR And XRD. *Int. J. Coal Geol.* **2021**, *247*, No. 103857.

(21) Wang, X.; Jiang, Y.; Zhou, G.; Wang, P.; Wang, R.; Zhao, L.; Chou, C.-L. Behavior of Minerals and Trace Elements During Natural Coking: A Case Study of An Intruded Bituminous Coal in The Shuoli Mine, Anhui Province, China. *Energ Fuel.* **2015**, *29*, 4100−4113.

(22) Song, X.; Ma, H.; Saalidong, B. M.; Li, K. Petrography, Mineralogy, And Geochemistry of Thermally Altered Coal in The Tashan Coal Mine, Datong Coalfield, China. *Minerals.* **2021**, *11*, 1024.

(23) Kisch, H. J.; Taylor, G. H. Metamorphism and Alteration Near an Intrusive-Coal Contact. *Econ Geol.* **1966**, *61*, 343−361.

(24) Ward, C. R.; Warbrooke, P. R.; Roberts, F. I. Geochemical and Mineralogical Changes in A Coal Seam Due to Contact Metamorphism, Sydney Basin, New South Wales, Australia. *Int. J. Coal Geol.* **1989**, *11*, 105−125.

(25) Rimmer, S. M.; Yoksoulian, L. E.; Hower, J. C. Anatomy of An Intruded Coal, I: Effect of Contact Metamorphism on Whole-Coal Geochemistry, Springfield (No. 5) (Pennsylvanian) Coal, Illinois Basin. *Int. J. Coal Geol.* **2009**, *79*, 74−82.

(26) Wang, X.; Wang, S.; Hao, C.; Zhao, Y.; Song, X. Quantifying Orientation and Curvature in HRTEM Lattice Fringe Micrographs of Naturally Thermally Altered Coals: New Insights from A Structural Evolution Perspective. *Fuel* **2022**, *309*, No. 122180.

(27) Zhao, Y.; Wang, S.; Liu, Y.; Song, X.; Chen, H.; Zhang, X.; Lin, Y.; Wang, X. Molecular Modeling and Reactivity of Thermally Altered Coals by Molecular Simulation Techniques. *Energ Fuel.* **2021**, *35*, 15663−15674.

(28) Chen, H.; Wang, S.; Tang, Y.; Zeng, F.; Schobert, H. H.; Zhang, X. Aromatic Cluster and Graphite-Like Structure Distinguished by

HRTEM in Thermally Altered Coal and Their Genesis. *Fuel.* **2021**, *292*, No. 120373.

(29) Chen, H.; Wang, S.; Zhang, X.; Zhao, Y.; Zhang, H. A Study of Chemical Structural Evolution of Thermally Altered Coal and Its Effect on Graphitization. *Fuel* **2021**, *283*, No. 119295.

(30) Stobinski, L.; Lesiak, B.; Kövér, L.; Tóth, J.; Biniak, S.; Trykowski, G.; Judek, J. Multiwall Carbon Nanotubes Purification and Oxidation by Nitric Acid Studied by The FTIR And Electron Spectroscopy Methods. *J. Alloy. Compd.* **2010**, *501*, 77–84.

(31) Li, W.; Zhu, Y.; Chen, S.; You, Z. Research on The Structural Characteristics of Vitrinite in Different Coal Ranks. *Fuel* **2013**, *7*, 647–652.

(32) Jiang, Y.; Zong, P.; Tian, B.; Xu, F.; Tian, Y.; Qiao, Y.; Zhang, J. Pyrolysis Behaviors and Product Distribution of Shenmu Coal at High Heating Rate: A Study Using TG-FTIR and Py-GC/MS. *Energ Convers Manage.* **2019**, *179*, 72–80.

(33) He, X.; Liu, X.; Nie, B. FTIR and Raman Spectroscopy Characterization of Functional Groups in Various Rank Coals. *Fuel* **2017**, *206*, 555–563.

(34) Chen, C.; Tang, Y.; Guo, X. Comparison of Structural Characteristics of High-Organic-Sulfur and Low-Organic-Sulfur Coal of Various Ranks Based on FTIR and Raman Spectroscopy. *Fuel.* **2022**, *310*, No. 122362.

(35) Tamuly, J.; Bhattacharjya, D.; Saikia, B. K. Graphene/Graphene Derivatives from Coal, Biomass, and Wastes: Synthesis, Energy Applications, and Perspectives. *Energ Fuel.* **2022**, *36*, 12847–12874.

(36) Xu, J.; Tang, H.; Su, S.; Liu, J.; Han, H.; Zhang, L.; Xu, K.; Wang, Y.; Hu, S.; Zhou, Y.; Xiang, J. Micro-Raman Spectroscopy Study of 32 Kinds of Chinese Coals: Second-Order Raman Spectrum and Its Correlations with Coal Properties. *Energ Fuel.* **2017**, *31*, 7884–7893.

(37) Wang, Y.; Alsmeyer, D. C.; McCreery, R. L. Raman Spectroscopy of Carbon Materials: Structural Basis of Observed Spectra. *Chem. Mater.* **1990**, *2*, 557–563.

(38) Guedes, A.; Valentim, B.; Prieto, A. C.; Noronha, F. Raman Spectroscopy of Coal Macerals and Fluidized Bed Char Morphotypes. *Fuel.* **2012**, *97*, 443–449.

(39) Chen, S.; Wu, D.; Liu, G.; Sun, R. Raman Spectral Characteristics of Magmatic-Contact Metamorphic Coals from Huainan Coalfield, China. *Spectrochim. Acta A* **2017**, *171*, 31–39.

(40) Li, K.; Rimmer, S. M.; Presswood, S. M.; Liu, Q. Raman Spectroscopy of Intruded Coals from The Illinois Basin: Correlation with Rank and Estimated Alteration Temperature. *Int. J. Coal Geol.* **2020**, *219*, No. 103369.

(41) Chen, H.; Wang, S.; Deng, J.; Zhang, X.; Liu, Y.; Li, X. Petrologic Characteristics and Chemical Structures of Macerals in A Suite of Thermally Altered Coals by Confocal Raman. *Energ Fuel.* **2021**, *6*, 33409–33418.

(42) Zhang, J.; Zheng, C.; Ren, D.; Chou, C.-L.; Liu, J.; Zeng, R.; Wang, Z.; Zhao, F.; Ge, Y. Distribution of Potentially Hazardous Trace Elements in Coals from Shanxi Province, China. *Fuel.* **2004**, *83*, 129–135.

(43) Niu, X.; Chen, B.; Feng, G.; Liu, F.; Yang, J. Origin of Lamprophyres from The Northern Margin of The North China Craton: Implications for Mantle Metasomatism. *J. Geol Soc. London.* **2017**, *174*, 353–364.

(44) Song, X.; Li, K.; Ma, H.; Liu, D.; Zhao, J.; Zhou, J. Characteristics of an Altered Diabase Dike in A Coal Seam: A Case Study From The Datong Coalfield, Shanxi, China. *Geofluids* **2020**, *3*, 1–14.

(45) Luo, P.; Tang, Y.; Li, R.; Ju, M. Effects of Minerals Type and Content on the Synthetic Graphitization of Coal: Insights from the Mixture of Minerals and Anthracite with Varied Rank. *Minerals.* **2023**, *13* (8), 1024.

(46) Bishop, M.; Ward, D. L. The Direct Determination of Mineral Matter in Coal. *Fuel* **1958**, *37*, 191–200.

(47) Nyathi, M. S.; Clifford, C. B.; Schobert, H. H. Characterization of Graphitic Materials Prepared from Different Rank Pennsylvania Anthracites. *Fuel.* **2013**, *114*, 244–250.

(48) Rodrigues, S.; Suárez-Ruiz, M.; Flores, D.; Camean, I.; García, A. B. Development of Graphite-Like Particles from The High Temper-ature Treatment of Carbonized Anthracites. *Int. J. Coal Geol.* **2011**, *85*, 219–226.

(49) Hummers, W. S.; Offeman, R. E. Preparation of Graphitic Oxide. *J. Am. Chem. Soc.* **1958**, *80*, 1339.

(50) Botas, C.; Álvarez, P.; Blanco, P.; Granda, M.; Blanco, C.; Santamaría, R.; Romasanta, L. J.; Verdejo, R.; López-Manchado, M. A.; Menéndez, R. Graphene Materials with Different Structures Prepared from The Same Graphite by The Hummers and Brodie Method. *Carbon* **2013**, *5*, 156–164.

(51) *ASTM D2798–21, Standard Test Method for Microscopical Determination of the Vitrinite Reflectance of Coal*; ASTM International: West Conshohocken, PA, 2021.

(52) *ASTM D3173/D3173M-17a, Standard Test Method for Moisture in the Analysis Sample of Coal and Coke, West Conshohocken*; ASTM International: West Conshohocken, PA, 2017.

(53) *ASTM D3174–12(2018) e1, Standard Test Method for Ash in the Analysis Sample of Coal and Coke from Coal*; ASTM International: West Conshohocken, PA, 2018.

(54) *ASTM D3175–20, Standard Test Method for Volatile Matter in the Analysis Sample of Coal and Coke*; ASTM International: West Conshohocken, PA, 2020.

(55) *ASTM D5373-21, Standard Test Methods for Determination of Carbon, Hydrogen and Nitrogen in Analysis Samples of Coal and Carbon in Analysis Samples of Coal and Coke*; ASTM International: West Conshohocken, PA, 2021.

(56) *ASTM D3177–02. Test Method for Total Sulfur in the Analysis Sample of Coal and Coke from Coal*; ASTM International: West Conshohocken, PA, 2011.

(57) Painter, P. C.; Snyder, R. W.; Starsinic, M.; Coleman, M. M.; Kuehn, D. W.; Davis, A. Concerning the Application of FTIR To the Study of Coal: A Critical Assessment of Band Assignment and The Application of Spectral Analysis Programs. *Appl. Spectrosc.* **1981**, *35*, 475–485.

(58) Geng, W. L.; Nakajima, T.; Takanashi, H.; Ohki, A. Analysis of Carboxyl Group in Coal and Coal Aromaticity by Fourier Transform Infrared (FT-IR) Spectrometry. *Fuel.* **2009**, *88*, 139–144.

(59) Ibarra, J.; Moliner, R.; Bonet, A. J. FT-I.R. Investigation on Char Formation During the Early Stages of Coal Pyrolysis. *Fuel.* **1994**, *73*, 918–924.

(60) Wang, S.; Tang, Y.; Schobert, H. H.; Guo, Y.; Su, Y. FTIR and ^{13}C NMR Investigation of Coal Component of Late Permian Coals from Southern China. *Energ Fuel.* **2011**, *25*, 5672–5677.

(61) Ahmed, M. A.; Blesa, M. J.; Juan, R.; Vandenberghe, R. E. Characterisation of An Egyptian Coal by Mossbauer and FT-IR Spectroscopy. *Fuel.* **2003**, *82*, 1825–1829.

(62) Manoj, B.; Narayanan, P. Study of Changes to The Organic Functional Groups of a High Volatile Bituminous Coal During Organic Acid Treatment Process by FTIR Spectroscopy. *J. Miner. Mater. Charact. Eng.* **2013**, *1*, 39–43.

(63) Ganz, H.; Kalkreuth, W. Application of Infrared Spectroscopy to The Classification of Kerogen Types and The Evaluation of Source Rock and Oil Shale Potentials. *Fuel* **1987**, *66*, 708–711.

(64) Guo, Y.; Bustin, R. M. Micro-FTIR Spectroscopy of Liptinite Macerals in Coal. *Int. J. Coal Geol.* **1998**, *36*, 259–275.

(65) Sun, X. The Investigation of Chemical Structure of Coal Macerals Via Transmitted-Light FT-IR Microspectroscopy. *Spectrochim. Acta A Mol. Biomol. Spectrosc.* **2005**, *62*, 557–564.

(66) Jiang, J.; Yang, W.; Cheng, Y.; Liu, Z.; Zhang, Q.; Zhao, K. Molecular Structure Characterization of Middle-High Rank Coal Via XRD, Raman And FTIR Spectroscopy: Implications For Coalification. *Fuel.* **2019**, *239*, 559–572.

(67) Zhou, Q.; Zhao, Z.; Zhang, Y.; Bo, M.; Zhou, A.; Qiu, J. Graphene Sheets from Graphitized Anthracite Coal: Preparation, Decoration, And Application. *Energy Fuels* **2012**, *26*, 5186–5192.

(68) Jawhari, T.; Roid, A.; Casado, J. Raman Spectroscopic Characterization of Some Commercially Available Carbon Black Materials. *Carbon.* **1995**, *33*, 1561–1565.

(69) Stankovich, S.; Dikin, D. A.; Piner, R. D.; Kohlhaas, K. A.; Kleinhammes, A.; Jia, Y.; Wu, Y.; Nguyen, S. T.; Ruoff, R. S. Synthesis of

Graphene-Based Nanosheets Via Chemical Reduction of Exfoliated Graphite Oxide. *Carbon.* **2007**, *45*, 1558−1565.

(70) Baysal, M.; Yürüm, A.; Yildiz, B.; Yürüm, Y. Structure of Some Western Anatolia Coals Investigated By FTIR, Raman, ¹³C Solid State NMR Spectroscopy and X-Ray Diffraction. *Int. J. Coal Geol.* **2016**, *163*, 166−176.

(71) Lin-Vien, D.; Colthup, N. B.; Fateley, W. G. G. J. *The handbook of infrared and Raman characteristic frequencies of organic molecules*; Academic Press: San Diego (Califonia, USA), 1991.

(72) Li, X.; Hayashi, J.; Li, C. FT-Raman Spectroscopic Study of The Evolution of Char Structure During the Pyrolysis of a Victorian Brown Coal. *Fuel.* **2006**, *85*, 1700−1707.

(73) Kelemen, S. R.; Fang, H. L. Maturity Trends in Raman Spectra from Kerogen and Coal. *Energ Fuel.* **2001**, *15*, 653−658.

(74) Hinrichs, R.; Brown, M. T.; Vasconcellos, M. A. Z.; Abrashev, M. V.; Kalkreuth, W. Simple Procedure for An Estimation of The Coal Rank Using Micro-Raman Spectroscopy. *Int. J. Coal Geol.* **2014**, *136*, 52−58.

(75) Schwan, J.; Ulrich, S.; Batori, V.; Ehrhardt, H.; Silva, S. R. P. Raman Spectroscopy on Amorphous Carbon Films. *J. Appl. Phys.* **1996**, *80*, 440−447.